Spatial Coherence in Near-Field Raman Scattering

Ryan Beams,[1] Luiz Gustavo Cançado,[2] Sang-Hyun Oh,[3] Ado Jorio,[2] and Lukas Novotny[4]
[1]Institute of Optics, University of Rochester, Rochester, New York 14627, USA
[2]Departamento de Física, Universidade Federal de Minas Gerais, Belo Horizonte, MG 30123-970, Brazil
[3]Department of Electrical and Computer Engineering, University of Minnesota, Minneapolis, Minnesota 55455, USA
[4]Photonics Laboratory, ETH Zürich, 8093 Zürich, Switzerland*
(Received 13 June 2014; published 28 October 2014)

Inelastic light scattering in crystals has historically been treated as a spatially incoherent process, giving rise to incoherent optical radiation. Here we demonstrate that Raman scattering can be spatially coherent, in which case it depends on the dimensionality and symmetry of the scatterer. Using near-field spectroscopy, we measure a correlation length of ~30 nm for the optical phonons in graphene, the results varying with vibrational symmetries and spatial confinement of the phonons.

DOI: 10.1103/PhysRevLett.113.186101 PACS numbers: 68.37.Uv, 63.22.Rc, 81.05.ue

In classical textbooks inelastic scattering, such as Raman scattering, is usually treated as a spatially incoherent process, that is, the response from different volume elements are added up [1,2]. Thus, the scattered fields from spatially distinct locations are considered to be uncorrelated, and the scattered signal, S, is then proportional to the volume of the scatterer, V. This is represented by the expression $S \propto V|\boldsymbol{\epsilon} \cdot \overleftrightarrow{\alpha}\mathbf{E}|^2$, where $\boldsymbol{\epsilon}$ is a unit vector defining the scattering polarization direction and $\overleftrightarrow{\alpha}$ is the polarizability of a volume element [1,2]. This formalism has been justified for macroscopic light-matter interactions because the correlation length L_c of material excitations, such as optical phonons, is typically on the order of tens of nanometers, one order of magnitude shorter than the wavelength of visible light. However, while correlation lengths significantly smaller than the wavelength λ are inaccessible in standard diffraction limited measurement schemes [3], they do play an important role in the near-field regime and cannot be neglected for scattering processes at the nanoscale [4–9]. Therefore, applications in nanotechnology demand quantitative knowledge of the correlation length of material excitations and the associated coherent properties of scattered light.

The scattered signal S at the location of the detector $\mathbf{r}_0$ from a material represented by a distribution of scattering dipoles $\mathbf{p}$ is calculated by [26]

$$\begin{aligned} S(\mathbf{r}_0) &\propto \langle \mathbf{E}_S^*(\mathbf{r}_0)\mathbf{E}_S(\mathbf{r}_0)\rangle \\ &= \int\int \overleftrightarrow{\mathbf{G}}^*(\mathbf{r}_0,\mathbf{r}_1)\overleftrightarrow{\mathbf{G}}(\mathbf{r}_0,\mathbf{r}_2)\langle \mathbf{p}^*(\mathbf{r}_1)\mathbf{p}(\mathbf{r}_2)\rangle d^3\mathbf{r}_1 d^3\mathbf{r}_2 \\ &= \int\int \langle \overleftrightarrow{\alpha}^*_{\mathbf{r}_1}\overleftrightarrow{\alpha}_{\mathbf{r}_2}\rangle [\overleftrightarrow{\mathbf{G}}(\mathbf{r}_0,\mathbf{r}_1)\mathbf{E}(\mathbf{r}_1)]^* \\ &\quad \times [\overleftrightarrow{\mathbf{G}}(\mathbf{r}_0,\mathbf{r}_2)\mathbf{E}(\mathbf{r}_2)] d^3\mathbf{r}_1 d^3\mathbf{r}_2, \end{aligned} \tag{1}$$

where $\overleftrightarrow{\mathbf{G}}$ is the Green's tensor and $\overleftrightarrow{\alpha}_{\mathbf{r}_i}$ is the polarizability tensor at location $\mathbf{r}_i$. We consider a linear relationship ($\mathbf{p} = \overleftrightarrow{\alpha}\mathbf{E}$) between dipole and local field. The expression $\langle \overleftrightarrow{\alpha}^*_{\mathbf{r}_1}\overleftrightarrow{\alpha}_{\mathbf{r}_2}\rangle$ accounts for the correlation between scattering dipoles $\mathbf{p}$ at positions $\mathbf{r}_1$ and $\mathbf{r}_2$. If the correlation length is negligible, the correlation function is a Dirac delta function $\delta(\mathbf{r}_1 - \mathbf{r}_2)$. As a consequence, the spatial coherence of scattered light is low. However, if the light-matter interaction volume becomes comparable to the correlation length we can no longer approximate $\langle \overleftrightarrow{\alpha}^*_{\mathbf{r}_1}\overleftrightarrow{\alpha}_{\mathbf{r}_2}\rangle$ by a delta function. Here we use a near-field Raman scattering scheme to experimentally demonstrate the importance of the correlation function $\langle \overleftrightarrow{\alpha}^*_{\mathbf{r}_1}\overleftrightarrow{\alpha}_{\mathbf{r}_2}\rangle$ in the scattered intensity. Using strongly localized light fields, we measure phonon correlation lengths in graphene of 30 ± 5 nm, which is more than an order of magnitude smaller than the excitation wavelength. Furthermore, we find that the spatial coherence of scattered light is strongly influenced by the symmetry of the phonon mode involved in the scattering process. The spatial coherence of phonons is of great importance for graphene electronics and has so far only been explored in the time and frequency domains [10–15]. Near-field Raman scattering can also be used to measure phonon correlations in polycrystalline and noncrystalline solids, where the correlation lengths are significantly shorter than in crystals. This opens new research directions for tip-enhanced Raman spectroscopy (TERS).

For a coherent process the strength of the scattered field depends on the symmetry of the vibrational mode, since the scattered fields from neighboring lattice points add constructively or destructively depending on the relative phase between the points. Beyond this, the dimensionality of the sample is also important since it determines the number of lattice points that are coherently added. The degree to which the fields from neighboring points interfere is determined by a spatial correlation function. Graphene is an excellent prototype material to study such correlations. Its three main Raman features span the different mode

symmetries and dimensionalities that are needed: the G ($\sim$1580 cm^{-1}) and G' band (also called 2D, centered at $\sim$2700 cm^{-1}) are allowed over the whole graphene lattice but they exhibit different symmetries [16,17]. The G band belongs to the E_{2g} irreducible representation in group theory, which means it is symmetric under a C_2 axis (180° rotation) [16]. The G' band belongs to the totally symmetric irreducible representation A_1', thus exhibiting the full C_6 (60° rotation) symmetry of graphene [16]. The third prominent band is the defect-induced D band ($\sim$1350 cm^{-1}), which is highly localized at graphene edges [18–21]. This Raman feature has the same symmetry as its overtone G' band, but unlike the two previous cases that are spread over the two-dimensional (2D) graphene lattice, the localization of the D band mimics a one-dimensional (1D) system. Therefore, graphene allows us to study the spatial coherence of the Raman process for different mode symmetries and dimensionalities.

Our experiments were performed with a near-field Raman microscope, as described in Refs. [22,23]. Figure 1(a) illustrates the measurement scheme and Fig. 1(b) shows a typical TERS image (G') of a single-layer graphene flake. As a comparison, the inset shows the confocal image of the same area of the flake. These images clearly show the improvement in signal and resolution in the near-field configuration. To better illustrate the TERS enhancement, spectra were acquired at the edge [black circle in Fig. 1(b)] and in the center of the flake [black square in Fig. 1(b)] with the tip down (red) and retracted (black), which are shown in top and bottom panels of Fig. 1(c), respectively. We do not observe any disorder-induced D band away from the edge, indicating that the flake is pristine.

In order to further study the TERS signal, hyperspectral line scans were acquired with and without the tip. In this case, the sample was scanned along a line perpendicular to the edge and at each spatial position a spectrum was acquired [Fig. 2(a)]. The resulting spectra were fit with Lorentzians and normalized by the tip-up values at each location. Figure 2(b) shows the results for the D band, indicating that the D band signal is greatly enhanced and highly localized at the edge to $\sim$40 nm. This provides a measurement of the tip radius, $r_{\mathrm{tip}} \approx 18 \pm 3$ nm. The width of the D band intensity profile is slightly larger than $2r_{\mathrm{tip}}$, due to a convolution of the near-field spot with the spatial extent of the D band ($\approx$ 4 nm). The latter corresponds to the distance from the graphene edge for which the D band is still Raman active and is determined by the coherence length (or phase-breaking length) of the excited electronic

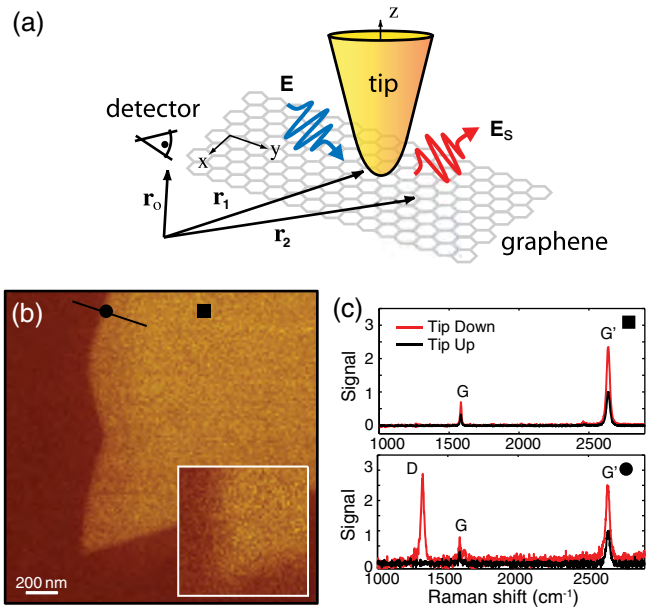

FIG. 1 (color online). TERS characterization of a graphene flake. (a) Sketch of the experiment. An incident electric field, $\mathbf{E}$, inelasically scatters off the graphene lattice creating the outgoing field $\mathbf{E}_s$. A gold tip is used to measure the correlations on the sample. (b) TERS image of the G' band of a single graphene flake. The black line indicates the location of the hyperspecral line scan in Fig. 2. Inset: confocal image of the same area with the color contrast scaled by ×3. (c) Raman spectra with (red) and without (black) the tip acquired in the center (top panel) and at the edge (bottom panel) of the flake. The locations are indicated by the black square and circle in (b), respectively.

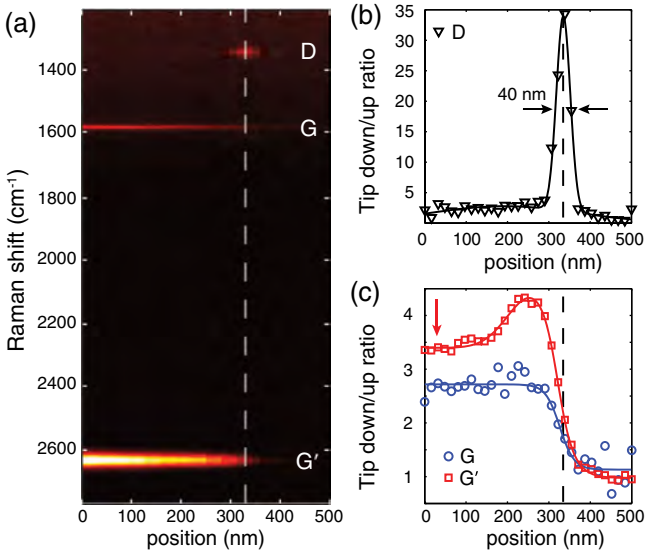

FIG. 2 (color online). TERS hyperspectral line scan acquired along the black line in Fig. 1(b). (a) Color map showing the intensities of the Raman bands as one moves from the inside (position equals 0 nm) to the outside of the flake (position equals 500 nm). The edge of the flake is indicated by the dashed line. (b), (c) Plots of the amplitudes for the D (black triangles), G (blue circles), and G' (red squares) bands from the hyperspectral line scan shown in (a). The tip-down spectra are normalized by the far-field value at each location. The D band profile is fit with two Gaussians: one for the confocal focus and one for the near-field signal. The bump near the edge in the G' band data is likely due to strain and dopants.

states [18–21]. The line scans of the G and G' bands look similar, being more intense when the near-field of the tip enters the graphene material, as shown in Fig. 2(c). However, there are important differences: the G' band shows a steeper signal increase at the graphene edge. Furthermore, away from the edge (red arrow), the measured enhancement for the G' band is larger than for the G band. The reduced enhancement of the G band compared to the G' band, together with the different signal steepness at the edge, provides evidence that both the spatial phonon correlations and the phonon mode symmetry impact the TERS signal.

The results in Fig. 2 demonstrate qualitatively that mode confinement and symmetry are important in Raman scattering. For a more quantitative analysis, the dependence of the Raman enhancement on the phonon correlation length should be studied as a function of the tip-sample separation. The theoretical dependence of the signal on the tip-sample separation (z_{ts}) is summarized in Fig. 3 for the D, G, and G' bands. The theoretical results are an extension of Refs. [24,25] and are described in detail in Ref. [26]. The D band signal is evaluated at the graphene edge, whereas the G and G' bands are evaluated in the interior of the flake. Figures 3(a) and 3(b) show tip-sample distance curves for two values of the phonon correlation length L_c: 0 and 50 nm, respectively. In the case of a spatially uncorrelated process ($L_c = 0$), the G and G' curves coincide [Fig. 3(a)]. However, due to the different dimensionality of the scattering domain (edge versus interior), the D band has a steeper tip-sample distance dependence (stronger enhancement). The distance dependence drops for all bands as L_c increases [Fig. 3(b)]. Most importantly, as L_c increases the G and G' signals become strikingly different, with the G band showing a markedly weaker enhancement. Note that the D and G' bands are both second-order scattering processes. Their excited electron-hole pairs are spatially confined to a few nanometers [19–21], which does not influence the phonon correlations measured in this work.

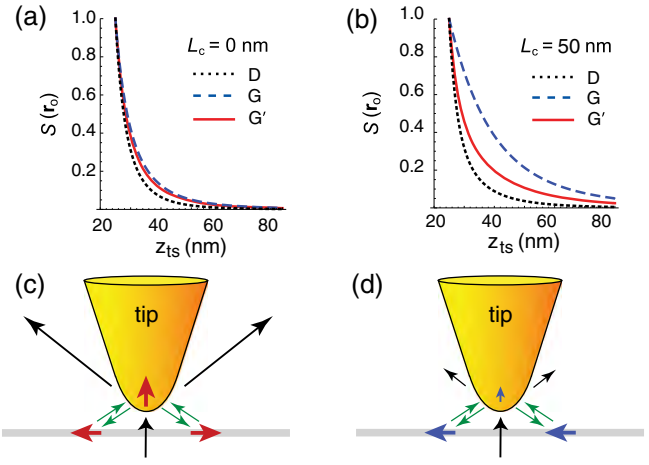

FIG. 3 (color online). Theoretical description of the TERS signal. (a),(b) Dependence of the signal on the tip-sample separation (z_{ts}) for the D, G, and G' bands. The curves are calculated with two different phonon correlation lengths: $L_c = 0$ nm and $L_c = 50$ nm. The signal $S(\mathbf{r}_o)$ is normalized to 1 for $z_{ts} = 25$ nm, which corresponds to the closest tip-sample distance. (c),(d) Sketches of the TERS process. The incident field induces a vertical dipole in the tip that interacts with the sample (green arrows), which in turn acts back on the tip at the Raman frequency (green arrows) before the fields are scattered out to the detector. The strength of the scattered signal depends on the relative phase of the induced dipoles in the sample (horizontal red and blue arrows). The emission dipoles on the sample add constructively for the G' band and destructively for the G band, as shown in (c),(d), respectively.

The deviation between the G and G' bands arises from the interaction between neighboring lattice points and provides theoretical evidence for interference effects associated with the coherence of the scattered field. This interference is illustrated in sketches of the TERS process shown in Figs. 3(c) and 3(d). The incident field (vertical black arrow) induces a vertical dipole in the tip. The fields from the tip induce dipoles in the sample (horizontal arrows), which then interact again with the tip by inducing a vertical dipole (at the Raman frequency) that scatters the Raman signal to the detector. The strength of the Raman signal depends on the relative phase of the dipoles induced in the sample. For the G' band the fields from the dipoles in the sample add constructively at the tip [Fig. 3(c)]. However, for the G band the fields destructively interfere, which reduces the Raman signal at the detector [Fig. 3(d)]. These theoretical curves indicate how nanoscale spatial correlations can be experimentally determined by measuring the distance dependence of the TERS signal.

To experimentally validate the theoretical predictions, we have measured the tip-sample distance dependence of three different Raman modes in graphene. The tip was positioned over the edge of a graphene flake and was retracted from the surface while Raman spectra were acquired for discrete tip-sample separations z_{ts}. The data were fit using Eq. (1), which was theoretically developed in Ref. [26]. The fitting parameters are the phonon correlation length L_c and the field enhancement factor $\tilde{f}_e$. The latter depends solely on the plasmonic properties of the tip. For the G' band $\tilde{f}_e$ primarily determines the steepness of the curve in the last 10–20 nm, whereas L_c strongly influences larger tip-sample separations. However, the G band is very sensitive to L_c even for short tip-sample separations due to the destructive interference at the tip. Figure 4(a) shows the approach curves for the D (black triangles), G (blue circles), and G' (red squares) bands. From the fits we find $L_c = 30 \pm 5$ nm and $\tilde{f}_e = 4.0$. r_{tip} was independently determined from the spatial confinement of the D band. The enhancement is clearly more modest for the G band than for the G' or D band, as expected due to the interference effect discussed above. The differences in the approach curves for distinct bands are better shown by

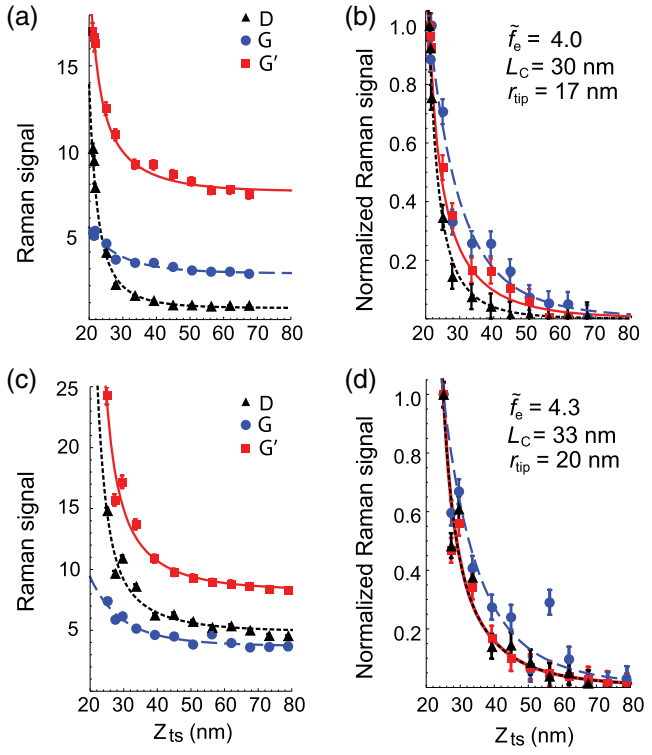

FIG. 4 (color online). Experimental tip-sample distance curves for the Raman D (black triangles), G (blue circles), and G' (red squares) bands of two graphene samples. Top row: acquired at the edge of a pristine graphene flake. Bottom row: ion bombarded flake with uniformly distributed defects. (a),(c) Amplitudes of the Raman bands. (b),(d) Normalized data from (a) and (b), respectively, with the far-field values subtracted. The data are overlayed with the theoretical curves evaluated in Ref. [26], and shown Fig. 3. The values for the enhancement factor ($\tilde{f}_e$), correlation length (L_c), and tip radius (r_{tip}) are indicated in the plots.

subtracting the far-field value (signal in absence of the tip) before normalizing, as shown in Fig. 4(b). The results clearly demonstrate that the D band has a stronger tip-sample distance dependence than the G and G' bands, and this difference is due to the fact that the edge behaves as a 1D scatterer. Furthermore, the G' band enhancement is stronger than for the G band for finite values of L_c, which is clearly seen in the measurement shown in Fig. 4(b). Note that we are measuring the phonon correlation length using the coherence properties of the Raman signal and we do not need to directly resolve L_c. However the size of the tip does influence the measurements. Each correlated area, A_c, on the sample has a well-defined phase, but the phase is random between different regions. As the tip size increases it interacts with a larger sample area and the degree of coherence depends on the number of A_c areas that are averaged (see the Supplemental Material [27]).

To further distinguish the roles of the mode symmetry versus sample dimensionality on the TERS signal, a defective flake was prepared by ion bombardment with an interdefect spacing of ~15 nm [19]. In this case, the D band is active everywhere on the 2D flake and no longer confined to the 1D edge. We acquired an approach curve in the center of this graphene flake and the results are shown in Figs. 4(c) and 4(d). It is evident that the enhancement for the D and G' bands is stronger than for the G band [Fig. 4(d)]. In addition, the approach curves for the D and G' bands are nearly identical. As discussed earlier the D and G' bands have A_1' symmetry, whereas the G band has E_{2g} symmetry. These results clearly show that the phonon symmetry significantly influences the near-field signal. From the fitting procedure, we find $L_c = 33 \pm 5$ nm and $\tilde{f}_e = 4.3$ for this data set, which is in good agreement with the measurement at the edge [Figs. 4(a) and 4(b)]. The similar values for L_c at the edge and away from the edge indicate that the phonon-edge scattering is not affecting the spatial coherence (see the Supplemental Material [27]).

Although coherence effects in inelastic light scattering have been neglected for decades, we find that near-field Raman scattering must be treated as a partially coherent process and that it is highly sensitive to the dimensionality and symmetry of the scatterer. While the importance of Raman spectroscopy for studying and characterizing nanostructures is well established [16,17], we demonstrate that this technique also provides access to spatial correlation functions, such as phonon coherence lengths. Recent studies have shown TERS with spatial resolutions of better than 1 nm [28,29], which brings TERS resolutions to the level of scanning tunneling microscopy. At this length scale coherence effects will completely dominate the measured signals in extended material systems. Furthermore, this technique opens the possibility of exploring the impacts of the substrate, carrier concentration, defect density, and temperature on phonon correlations.

A. J. acknowledges CAPES for supporting his stay at ETH. A. J. and L. G. C. acknowledge financial support from CNPq and FAPEMIG. L. N. acknowledges financial support by the U.S. Department of Energy (Grant No. DE-FG02-05ER46207) and the Swiss National Science Foundation (Grant No. 200021_149433).

[*] www.nano-optics.org
www.labns.com.br/en

[1] M. Cardona, in *Light Scattering in Solids II* (Springer, New York, 1982), pp. 19–178.
[2] W. Hayes and R. Loudon, *Scattering of Light by Crystals* (Wiley, New York, 1978).
[3] W. Carter and E. Wolf, J. Opt. Soc. Am. **65**, 1067 (1975).
[4] R. Carminati and J.-J. Greffet, Phys. Rev. Lett. **82**, 1660 (1999).
[5] A. V. Shchegrov, K. Joulain, R. Carminati, and J.-J. Greffet, Phys. Rev. Lett. **85**, 1548 (2000).
[6] H. Roychowdhury and E. Wolf, Opt. Lett. **28**, 170 (2003).
[7] A. Apostol and A. Dogariu, Phys. Rev. Lett. **91**, 093901 (2003).

[8] H. Roychowdhury and E. Wolf, J. Mod. Opt. **51**, 1603 (2004).
[9] B. T O'Callahan, W. E Lewis, A. C. Jones, and M. B. Raschke, Phys. Rev. B **89**, 245446 (2014).
[10] K. Kang, D. Abdula, D. G. Cahill, and M. Shim, Phys. Rev. B **81**, 165405 (2010).
[11] S. Berciaud, M. Y. Han, K. F. Mak, L. E. Brus, P. Kim, and T. F. Heinz, Phys. Rev. Lett. **104**, 227401 (2010).
[12] H. Wang *et al.*, Appl. Phys. Lett. **96**, 081917 (2010).
[13] S. Wu, W.-T. Liu, X. Liang, P. J. Schuck, F. Wang, Y. R. Shen, and M. Salmeron, Nano Lett. **12**, 5495 (2012).
[14] B. Y. Sun, Y. Zhou, and M. W. Wu, Phys. Rev. B **85**, 125413 (2012).
[15] G. D. Sanders, A. R. T Nugraha, K. Sato, J.-H. Kim, J. Kono, R. Saito, and C. J. Stanton, J. Phys. Condens. Matter **25**, 144201 (2013).
[16] A. Jorio, M. S. Dresselhaus, R. Saito, and G. Dresselhaus, *Raman Spectroscopy in Graphene Related System*, 1st ed. (Wiley-VCH, Weinheim, Germany, 2011).
[17] A. C. Ferrari and D. M. Basko, Nat. Nanotechnol. **8**, 235 (2013).
[18] C. Casiraghi, A. Hartschuh, H. Qian, S. Piscanec, C. Georgi, A. Fasoli, K. S. Novoselov, D. M. Basko, and A. C. Ferrari, Nano Lett. **9**, 1433 (2009).
[19] M. M. Lucchese, F. Stavale, E. H. Martins Ferreira, C. Vilani, M. V. O. Moutinho, Rodrigo B. Capaz, C. A. Achete, and A. Jorio, Carbon **48**, 1592 (2010).
[20] R. Beams, L. G. Cançado, and L. Novotny, Nano Lett. **11**, 1177 (2011).
[21] W. Su and D. Roy, J. Vac. Sci. Technol. B **31**, 041808 (2013).
[22] A. Hartschuh, Angew. Chem., Int. Ed. Engl. **47**, 8178 (2008).
[23] T. W. Johnson, Z. J. Lapin, R. Beams, N. C. Lindquist, S. G. Rodrigo, L. Novotny, and S.-H. Oh, ACS Nano **6**, 9168 (2012).
[24] L. G. Cançado, A. Jorio, A. Ismach, E. Joselevich, A. Hartschuh, and L. Novotny, Phys. Rev. Lett. **103**, 186101 (2009).
[25] R. V. Maximiano, R. Beams, L. Novotny, A. Jorio, and L. G. Cançado, Phys. Rev. B **85**, 235434 (2012).
[26] L. G. Cançado, R. Beams, A. Jorio, and L. Novotny, Phys. Rev. X **4**, 031054 (2014).
[27] See Supplemental Material at http://link.aps.org/supplemental/10.1103/PhysRevLett.113.186101 for additional approach curves and a discussion of the influence of the tip radius.
[28] R. Zhang *et al.*, Nature (London) **498**, 82 (2013).
[29] C. Chen, N. Hayazawa, and S. Kawata, Nat. Commun. **5**, 3312 (2014).

Supporting Information for Spatial Coherence in Near-Field Raman Scattering

Ryan Beams[1], Luiz Gustavo Cançado[2], Ado Jorio[2], and Lukas Novotny[3*]
[1] *Institute of Optics, University of Rochester, Rochester, NY 14627, USA.*
[2] *Departamento de Física, Universidade Federal de Minas Gerais, Belo Horizonte, MG 30123-970, Brazil*
[3] *Photonics Laboratory, ETH Zürich, 8093 Zürich, Switzerland.*
(Dated: August 26, 2014)

PACS numbers: 68.37.Uv, 81.05.ue, 63.22.Rc

NORMALIZED DISTANCE DEPENDENCE PLOTS

The approach curves from Fig. 4 of the main text have been re-plotted to further illustrate the differences between the various Raman bands. This difference is the direct result of the destructive interference for the G band and the constructive interference for the G′ and D bands. Figure S1(a)-(c) show the pristine flake (Fig. 4(a),(b) in the main text) and Fig. S1(d)-(f) show the damaged flake. In Fig. S1(a),(d) the raw counts are normalized by the maximum, which clearly shows the difference in the enhancement for the different bands. It is important to note that the data for the G′ and D bands overlap for the damaged flake (Fig S1(d)), which illustrates the importance of the mode symmetry. The ratio of the G′ band amplitude to the G band amplitude for the pristine flake is shown in Fig. S1(b). This ratio as well as the D band to G band ratio for the damaged flake are plotted in Fig. S1(e). Finally the data from Fig. 4(b),(d) of the main text is shown on a log-log scale in Fig. S1(c),(f). For the pristine flake the D band distance dependence is the steepest of the three bands as expected. The G′ band slope is slightly steeper than for the G as predicted from the theoretical model presented in Ref. 25. The slopes for the D and G′ bands for the damaged flake are identical and both are steeper than for the G band in agreement with the theory and the main text.

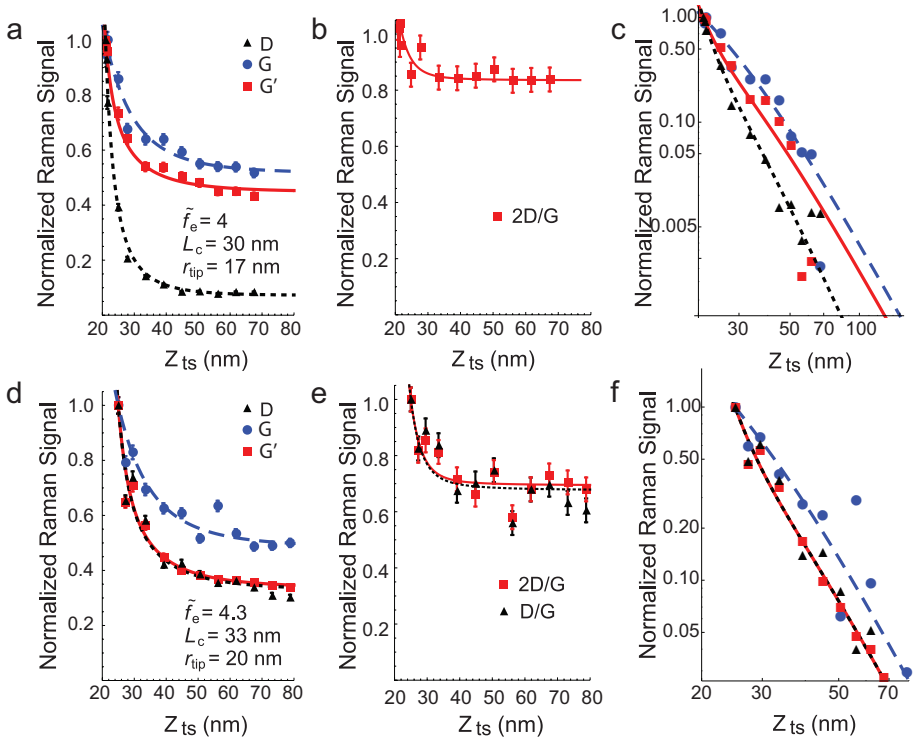

FIG. 1: Re-plots of the approach curves from Fig. 4 in main text. (a)-(c) Pristine flake. (d)-(f) Damaged flake. (a),(c) Data is normalized by the maximum counts. (b),(e) Ratios of the Raman bands. The lines in (b) and (e) are to guide the eye. (c),(f) Log-log plots of the data in (b) and (e), respectively.

ADDITIONAL DISTANCE DEPENDENCE MEASUREMENTS

Figure S2 shows approach curves acquired using a different tip in the center (Fig. S2(a)-(c)) and at the edge (Fig. S2(d)-(f)) of another flake, which is different from either flake shown in the main text. The G′ band shows more enhancement and a slightly steeper distance dependence in agreement with the data in the main text. From the fit, L_c =25 nm, which is in good agreement with Fig. 4 of the main text. Furthermore, the tip was slightly larger than the tips used in the main text (r_{tip} ≈30 nm), which caused the decreased enhancement factor and a more modest difference in the distance dependence of the G and G′ bands. This is expected for a larger tip, because the tip interacts with a larger sample volume and therefore the coherence effects are more averaged out. In other words, measurements with larger tips are partially coherent. Figure S2(a),(d) show the data normalized by the maximum counts and Fig. S2(b),(e) show the normalized data after subtracting the far-field counts. Finally, Fig. S2(c),(f) show the data from Fig. S2(b),(e) on a log-log scale. The log-log plot more clearly shows that the distance dependence of the D band is steeper. In addition, these plots show that the behavior of the G and G′ bands are the same in the center and at the edge of the flake. The differences between the G and G′ bands are subtle as expected for a partially coherent measurement using a larger tip.

INFLUENCE OF THE TIP RADIUS

Coherent scattering ($2 * r_{\mathrm{tip}} << L_{\mathrm{c}}$):
If the tip is significantly smaller than the correlation length the phonons in the entire interaction area have a well-defined phase. As a result at the tip we get purely coherent effects for the scattered photons.

Partially coherent scattering ($2 * r_{\mathrm{tip}} \approx L_{\mathrm{c}}$):

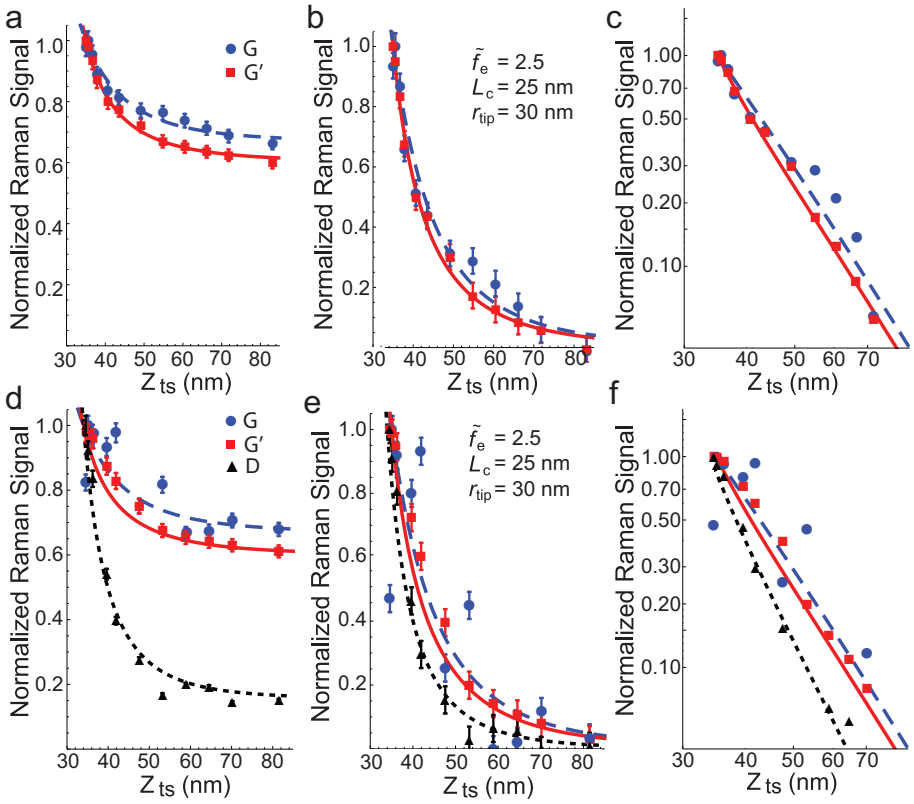

FIG. 2: Approach curve acquired on a pristine flake. (a)-(c) Acquired in the center of the flake. (d)-(f) Acquired at the edge of the flake. (a),(d) Signal normalized by the maximum (b),(e) Normalized values with the far-field value subtracted. (c),(f) Log-log plot of the data in (b) and (e), respectively.

As the tip gets bigger it interacts with a larger area on the sample and the phase of the phonons is not as well-defined. Therefore the result is partially coherent. This is analogous to decreasing the fringe visibility in a Young's double slit experiment.

Incoherent scattering ($2 * r_{\mathrm{tip}} >> L_{\mathrm{c}}$):
For a very large tip, each small area, A_{c}, on the sample still have a well-defined phase relationship, but there is no relationship between them. Since the tip is large it sums over many A_{c} areas. The random phase between each area averages out the coherence effects.

---

* URL: `www.nano-optics.org`